Experimental Section

Synthesis of D-BN

100 mg of as-received BN nanoplates were exfoliated to BN nanosheets in 50 mL of absolute ethyl alcohol under ultrasonication for 5 h. The obtained BN nanosheets were collected by centrifugation, washed three times with deionized water/ethanol and vacuum-dried overnight. The dried BN nanosheets were then subjected to Ar plasma treatment for 10 min in a plasma system (13.56 MHz) to obtain D-BN.

Electrochemical experiment

Electrochemical measurements were conducted under ambient conditions on a CHI-760E electrochemical workstation. The graphite rod, Ag/AgCl, and CC-loaded catalyst served as the reference, counter, and working electrodes, respectively. All potentials were referenced to reversible hydrogen electrode (RHE) by E (V vs. RHE) = E (V vs. Ag/AgCl) + 0.198 V + 0.059 × pH. The electrocatalytic NORR measurements were conducted within a gas-tight H-cell, using NO-saturated 0.5 M Na_2SO_4 electrolyte. Before NRR testing, the feeding gases were purified using two glass bubblers filled with 4 M KOH solution[1]. Furthermore, the cathodic compartment was flushed with Ar for a minimum of 30 minutes to eliminate any remaining oxygen. Throughout the NRR electrolysis process, a continuous flow of NO (99.9%) gas was introduced into the cathodic chamber at a rate of 20 mL min^{-1}. Subsequent to an hour of electrolysis, both the aqueous and gaseous products were identified using colorimetric methods and gas chromatography (GC), respectively.

Determination of NH_3

The generated NH_3 was determined by an indophenol blue method[2]. Typically, 0.5 mL of electrolyte was extracted from the electrochemical reaction vessel and subsequently diluted tenfold with deionized water. Then 2 mL of diluted solution was removed into a clean vessel followed by sequentially adding NaOH solution (2 mL, 1 M) containing $C_7H_6O_3$ (5 wt.%) and $C_6H_5Na_3O_7$ (5 wt.%), NaClO (1 mL, 0.05 M), and $C_5FeN_6Na_2O$ (0.2 mL, 1wt.%) aqueous solution. After incubation for 2 hours at room temperature. The mixed solution was measured in UV-Vis at 655 nm. The

concentration-absorbance curves were calibrated using a range of concentrations in a standard NH_4Cl solution. Subsequently, the NH_3 yield rate and Faradaic efficiency (FE_{NH3}) were calculated using the following equation:

$$NH_3 \text{ yield} = (c \times V) / (17 \times t \times A) \quad (1)$$

Faradaic efficiency was calculated by the following equation:

$$FE_{NH3} = (5 \times F \times c \times V) / (17 \times Q) \times 100\% \quad (2)$$

where c (μg mL^{-1}) is the measured NH_3 concentration, V (mL) is the volume of electrolyte in the cathode chamber, t (s) is the electrolysis time and A is the surface area of CC (1×1 cm^2), F (96500 C mol^{-1}) is the Faraday constant, Q (C) is the total quantity of applied electricity.

Determination of N_2H_4

N_2H_4 in electrolyte was quantitatively determined by a Watt and Chrisp method[3]. To prepare the coloring solution, a combination of 300 mL C_2H_5OH, 5.99 g $C_9H_{11}NO$, and 30 mL HCl was mixed. Subsequently, 5 mL of the coloring solution was introduced to 5 mL of the electrolyte. After the incubation for 20 min at room temperature, the mixed solution was subjected to UV-vis measurement using the absorbance at 455 nm wavelength. The concentration-absorbance curve is calibrated by a series of concentrations of standard N_2H_4 solutions.

Characterizations

X-ray diffraction (XRD) was performed on a Rigaku D/max 2400 diffractometer. Transmission electron microscopy (TEM) and selected area electron diffraction (SAED) were performed on a Tecnai G^2 F20 microscope. X-ray photoelectron spectroscopy (XPS) analysis was collected on a PHI 5702 spectrometer. Electron spin resonance (EPR) spectra were recorded on a Bruker EPR-300 spectrometer.

Calculation details

Spin-polarized density functional theory (DFT) calculations were carried out using the Cambridge sequential total energy package (CASTEP) with projector augmented wave pseudopotentials. The Perdew-Burke-Ernzerhof (PBE) generalized gradient approximation (GGA) functional was used for the exchange-correlation potential. The van der Waals interaction was described by using the empirical

correction in Grimme's scheme (DFT+D). During the geometry optimization, the electron wave functions were expanded using plane waves with a cutoff energy of 470 eV. The convergence tolerance was set to be 1.0×10^{-5} eV for energy and 0.02 eV $Å^{-1}$ for force. The 3 × 3 × 1 Monkhorst-Pack mesh was used in Brillouin zone sampling. BN (001) was modeled by a 2× 2 supercell, and a vacuum region of 15 Å was used to separate adjacent slabs.

The adsorption energy (ΔE) is defined as[4]

$$\Delta E = E_{\text{ads/slab}} - E_{\text{ads}} - E_{\text{slab}} \quad (3)$$

where $E_{\text{ads/slab}}$, E_{ads} and E_{slab} are the total energies for adsorbed species on slab, adsorbed species and isolated slab, respectively.

The Gibbs free energy (ΔG, 298 K) of reaction steps is calculated by[4]

$$\Delta G = \Delta E + \Delta ZPE - T\Delta S \quad (4)$$

where ΔE is the adsorption energy, ΔZPE is the zero-point energy difference and $T\Delta S$ is the entropy difference between the gas phase and adsorbed state.

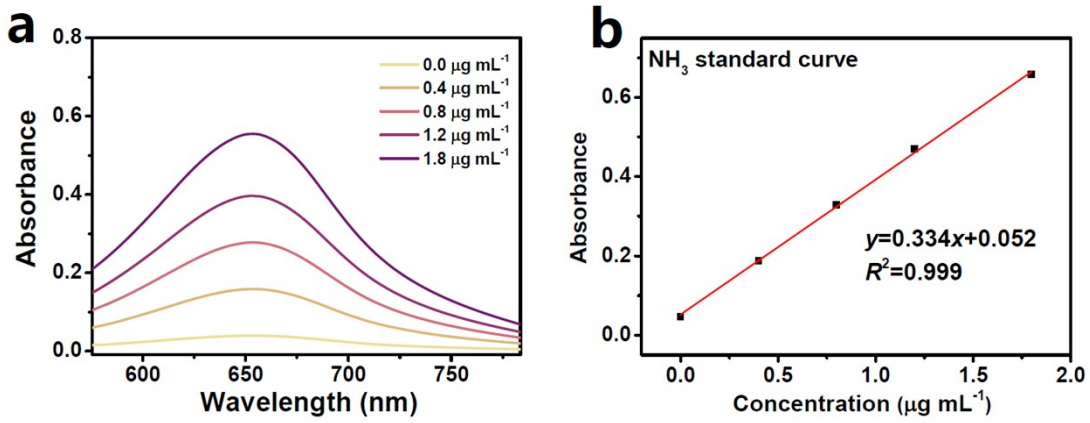

Fig. S1. (a) UV-vis absorption spectra of NH_4^+ assays after incubated for 2 h at ambient conditions. (b) Calibration curve used for the calculation of NH_3 concentrations.

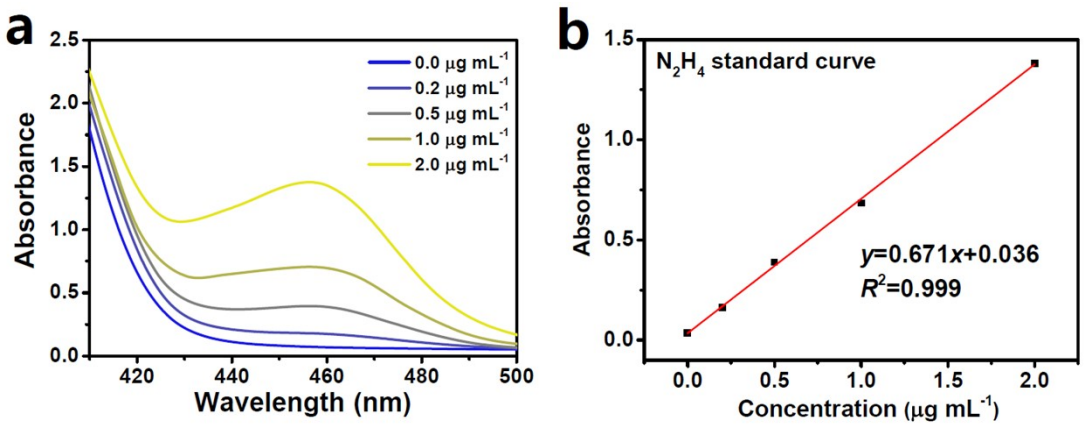

Fig. S2. (a) UV-vis absorption spectra of N_2H_4 assays after incubated for 20 min at ambient conditions. (b) Calibration curve used for calculation of N_2H_4 concentrations.

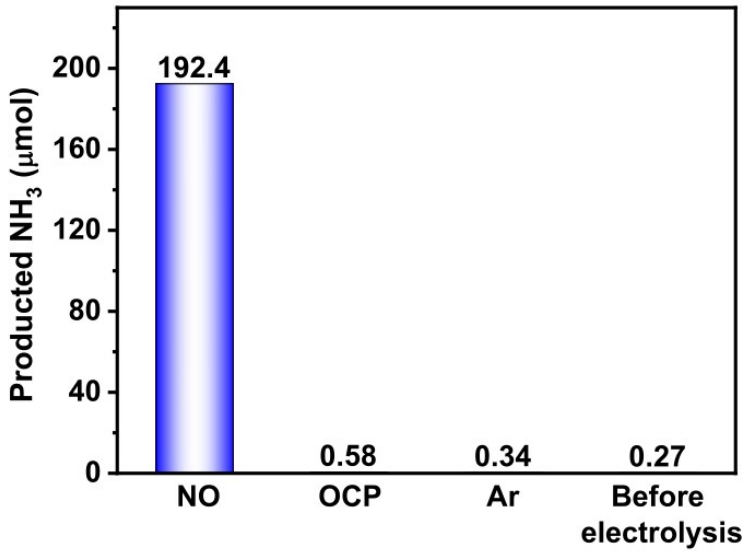

Fig. S3. Amounts of produced NH_3 over D-BN under different conditions: (1) electrolysis in NO-saturated solution at -0.7 V, (2) electrolysis in Ar-saturated solution at -0.7 V, (3) electrolysis in NO_2^--containing solution at open-circuit potential (OCP), (4) before electrolysis.

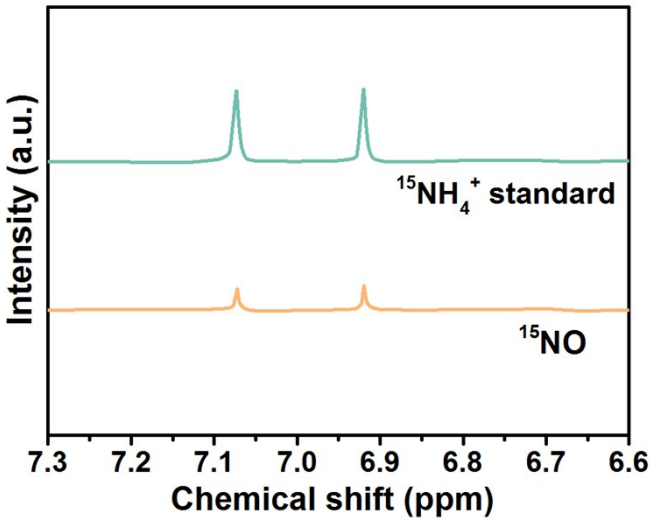

Fig. S4. ^{1}H NMR spectra of $^{15}NH_4^+$ standard sample and those fed by ^{15}NO after NORR electrolysis on D-BN at -0.7 V

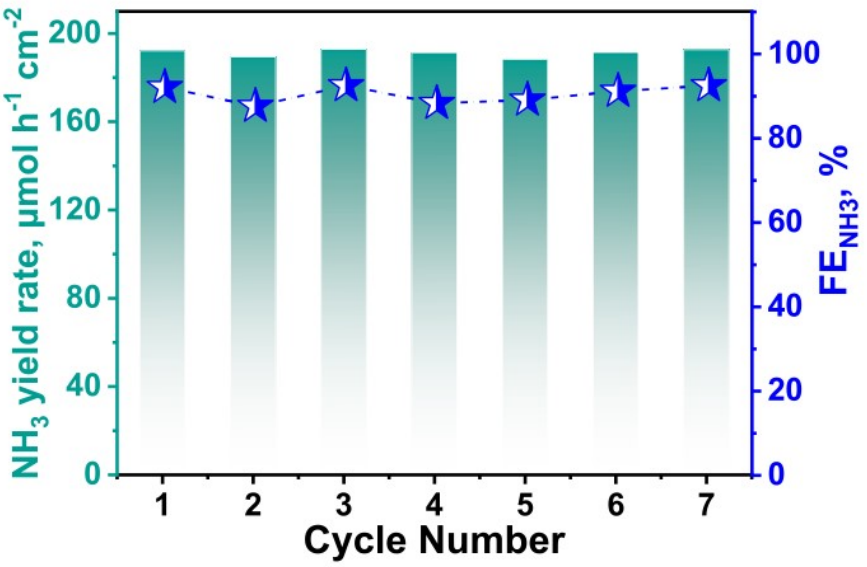

Fig. S5. Cycling test of D-BN at -0.7 V.

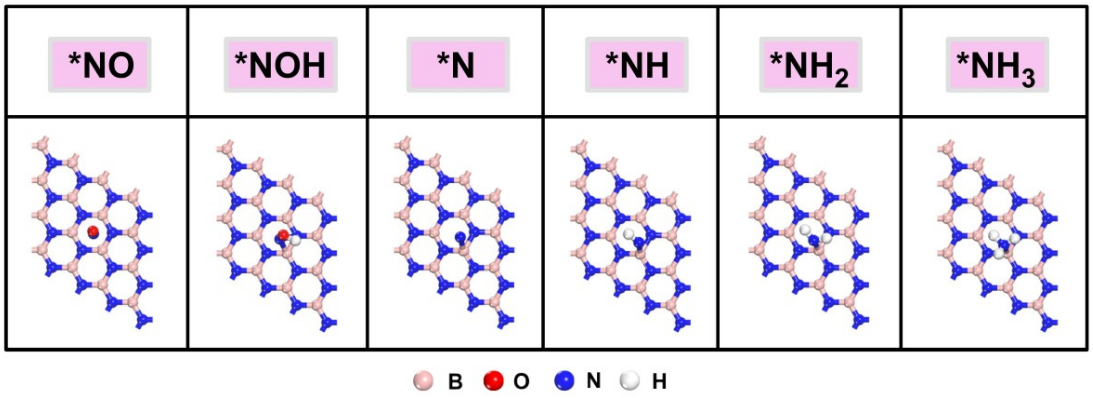

Fig. S6. Optimized structures of the reaction intermediates on pristine BN.

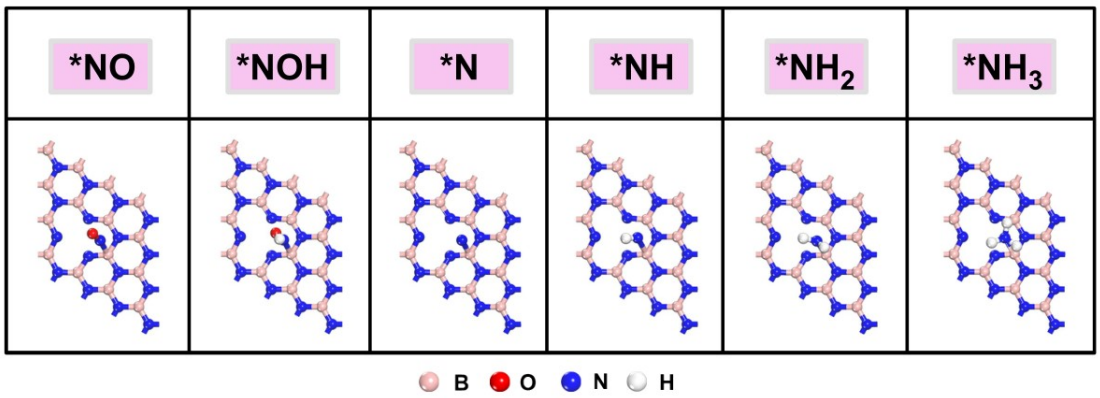

Fig. S7. Optimized structures of the reaction intermediates on D-BN.

Table S1. Comparison of the optimum NH_3 yield rate and NH_3-Faradic efficiency (FE_{NH3}) for recently reported NORR electrocatalysts at ambient conditions.

Catalyst	Electrolyte	NH_3 yield rate ($\mu mol\ h^{-1}\ cm^{-2}$)	FE_{NH3} (%)	Potential (V vs. RHE)	Ref.
NiO/TM	0.1 M Na_2SO_4	125.3	90	-0.6	[5]
Ni@NC	0.1 M HCl	34.6	72.3	0.16	[6]
Bi NDs	0.1 M Na_2SO_4	70.2	89.2	-0.5	[7]
$Cu_2O@CoMN_2O_4$	0.1 M Na_2SO_4	94.18	75.05	-0.9	[8]
CoS_{1-x}	0.2 M Na_2SO_4	44.67	53.62	-0.4	[9]
RuGa	0.1 M K_2SO_4	160.3	72.3	-0.2	[10]
NiFe-LDH	0.2 M Li_2SO_4	112	82	-0.7	[11]
a-$B_{2.6}C@TiO_2$/Ti	0.1 M Na_2SO_4	216.4	87.6	-0.9	[12]
$Ru_{0.05}Cu_{0.95}$	0.05 M Na_2SO_4	17.68	64.9	-0.5	[13]
HCNF	0.2 M Na_2SO_4	22.35	88.33	-0.6	[14]
Ni_2P/CP	0.1 M HCl	33.47	76.9	-0.2	[15]
CoP/TM	0.2 M Na_2SO_4	47.22	88.3	-0.2	[16]
D-BN	**0. 5 M Na_2SO_4**	**192.4**	**92.1**	**-0.7**	**This work**

References

[1]. L. Zhang, J. Liang, Y. Wang, T. Mou, Y. Lin, L. Yue, T. Li, Q. Liu, Y. Luo, N. Li, B. Tang, Y. Liu, S. Gao, A. A. Alshehri, X. Guo, D. Ma and X. Sun, *Angew. Chem. Int. Edit.*, 2021, **60**, 25263-25268.

[2]. P. Li, Z. Jin, Z. Fang and G. Yu, *Energy Environ. Sci.*, 2021, **14**, 3522-3531.

[3]. G. W. Watt and J. D. Chrisp, *Anal. Chem.*, 1952, **24**, 2006-2008.

[4]. Y. Zhang, J. Xiang, K. Chen, Y.-L. Guo, D. Ma and K. Chu, *Chem. Commun.*, 2023, **59**, 8961-8964.

[5]. P. Liu, J. Liang, J. Wang, L. Zhang, J. Li, L. Yue, Y. Ren, T. Li, Y. Luo, N. Li, B. Tang, Q. Liu, A. M. Asiri, Q. Kong and X. Sun, *Chem. Commun.*, 2021, **57**, 13562-13565.

[6]. S. Sethuram Markandaraj, T. Muthusamy and S. Shanmugam, *Adv. Sci.*, 2022, **9**, 2201410.

[7]. Y. Lin, J. Liang, H. Li, L. Zhang, T. Mou, T. Li, L. Yue, Y. Ji, Q. Liu, Y. Luo, N. Li, B. Tang, Q. Wu, M. S. Hamdy, D. Ma and X. Sun, *Mater. Today Phys.*, 2022, **22**, 100611.

[8]. C. Bai, S. Fan, X. Li, Z. Niu, J. Wang, Z. Liu and D. Zhang, *Adv. Funct. Mater.*, 2022, **32**, 2205569.

[9]. L. Zhang, Q. Zhou, J. Liang, L. Yue, T. Li, Y. Luo, Q. Liu, N. Li, B. Tang, F. Gong, X. Guo and X. Sun, *Inorg. Chem.*, 2022, **61**, 8096-8102.

[10]. H. Zhang, Y. Li, C. Cheng, J. Zhou, P. Yin, H. Wu, Z. Liang, J. Zhang, Q. Yun, A.-L. Wang, L. Zhu, B. Zhang, W. Cao, X. Meng, J. Xia, Y. Yu and Q. Lu, *Angew. Chem. Int. Ed.*, 2023, **62**, e202213351.

[11]. G. Meng, T. Wei, W. Liu, W. Li, S. Zhang, W. Liu, Q. Liu, H. Bao, J. Luo and X. Liu, *Chem. Commun.*, 2022, **58**, 8097-8100.

[12]. J. Liang, P. Liu, Q. Li, T. Li, L. Yue, Y. Luo, Q. Liu, N. Li, B. Tang, A. A. Alshehri, I. Shakir, P. O. Agboola, C. Sun and X. Sun, *Angew. Chem. Int. Ed.*, 2022, **61**, e202202087.

[13]. J. Shi, C. Wang, R. Yang, F. Chen, N. Meng, Y. Yu and B. Zhang, *Sci. China Chem.*, 2021, **64**, 1493-1497.

[14]. L. Ouyang, Q. Zhou, J. Liang, L. Zhang, L. Yue, Z. Li, J. Li, Y. Luo, Q. Liu, N. Li, B. Tang, A. Ali Alshehri, F. Gong and X. Sun, *J. Colloid Interf. Sci.*, 2022, **616**, 261-267.

[15]. T. Mou, J. Liang, Z. Ma, L. Zhang, Y. Lin, T. Li, Q. Liu, Y. Luo, Y. Liu, S. Gao, H. Zhao, A. M. Asiri, D. Ma and X. Sun, *J. Mater. Chem. A*, 2021, **9**, 24268-24275.

[16]. J. Liang, W.-F. Hu, B. Song, T. Mou, L. Zhang, Y. Luo, Q. Liu, A. A. Alshehri, M. S. Hamdy, L.-M. Yang and X. Sun, *Inorg. Chem. Front.*, 2022, **9**, 1366-1372.